Title

Attosecond transient absorption instrumentation for thin film materials: Phase transitions, heat dissipation, signal stabilization, timing correction, and rapid sample rotation

Journal

Review of Scientific Instruments, 89(1)

ISSN

0034-6748

Authors

Jager, Marieke F
Ott, Christian
Kaplan, Christopher J
et al.

Publication Date

2018

DOI

10.1063/1.4994041

Peer reviewed

Attosecond transient absorption instrumentation for thin film materials: Phase transitions, heat dissipation, signal stabilization, timing correction, and rapid sample rotation

Marieke F. Jager, Christian Ott, Christopher J. Kaplan, Peter M. Kraus, Daniel M. Neumark, and Stephen R. Leone

Citation: Review of Scientific Instruments **89**, 013109 (2018);
View online: https://doi.org/10.1063/1.4994041
View Table of Contents: http://aip.scitation.org/toc/rsi/89/1
Published by the American Institute of Physics

REVIEW OF SCIENTIFIC INSTRUMENTS **89**, 013109 (2018)

Attosecond transient absorption instrumentation for thin film materials: Phase transitions, heat dissipation, signal stabilization, timing correction, and rapid sample rotation

Marieke F. Jager,[1] Christian Ott,[1,2,a)] Christopher J. Kaplan,[1] Peter M. Kraus,[1] Daniel M. Neumark,[1,3,b)] and Stephen R. Leone[1,2,3,b)]
[1]*Department of Chemistry, University of California, Berkeley, California 94720, USA*
[2]*Department of Physics, University of California, Berkeley, California 94720, USA*
[3]*Chemical Sciences Division, Lawrence Berkeley National Laboratory, Berkeley, California 94720, USA*

(Received 3 July 2017; accepted 21 December 2017; published online 23 January 2018)

We present an extreme ultraviolet (XUV) transient absorption apparatus tailored to attosecond and femtosecond measurements on bulk solid-state thin-film samples, specifically when the sample dynamics are sensitive to heating effects. The setup combines methodology for stabilizing sub-femtosecond time-resolution measurements over 48 h and techniques for mitigating heat buildup in temperature-dependent samples. Single-point beam stabilization in pump and probe arms and periodic time-zero reference measurements are described for accurate timing and stabilization. A hollow-shaft motor configuration for rapid sample rotation, raster scanning capability, and additional diagnostics are described for heat mitigation. Heat transfer simulations performed using a finite element analysis allow comparison of sample rotation and traditional raster scanning techniques for 100 Hz pulsed laser measurements on vanadium dioxide, a material that undergoes an insulator-to-metal transition at a modest temperature of 340 K. Experimental results are presented confirming that the vanadium dioxide (VO_2) sample cannot cool below its phase transition temperature between laser pulses without rapid rotation, in agreement with the simulations. The findings indicate the stringent conditions required to perform rigorous broadband XUV time-resolved absorption measurements on bulk solid-state samples, particularly those with temperature sensitivity, and elucidate a clear methodology to perform them. *Published by AIP Publishing.* https://doi.org/10.1063/1.4994041

I. INTRODUCTION

Many solid-state materials have properties that are strongly temperature-dependent. In the most dramatic cases, solid-state phase transitions can result in sudden change of electronic, optical, or magnetic properties, which can be highly applicable for next-generation electronics.[1–3] Colossal magneto-resistance,[4] superconductivity,[5] and insulator-to-metal phase transitions[6,7] are examples that have already been integrated into prototype photonic switches and other devices.[8–10] As the engineering of these systems becomes more feasible, questions arise about the ultimate limits of such devices. Namely, it is important to understand how small they can be made and how quickly they can operate. To investigate the ultimate speed of these material properties, pulsed laser experiments are performed in various pump-probe geometries. Data are typically acquired by averaging over many laser pulses, where the measurement is repeated many times per second. However, heat buildup between laser pulses can be a significant impediment to measuring intrinsic material properties, especially if the material exhibits a phase transition driven by temperature. Heat mitigation problems are particularly enhanced under vacuum conditions where convective cooling is suppressed, which can be the case, for example, in experiments based on photoemission, soft x-ray, and extreme ultraviolet (XUV) measurements.

This work focuses on the emerging field of attosecond extreme ultraviolet measurements[11] and presents an apparatus for performing all-optical visible-pump XUV-probe transient absorption measurements on the bulk properties of freestanding thin-film solid-state samples, with emphasis on materials for which the response is strongly temperature-dependent, such as those that exhibit thermally induced phase transitions. Pulsed XUV sources are produced in a tabletop setting via high-harmonic generation (HHG),[12,13] a process that inherently creates attosecond pulse trains from which a single pulse can be isolated.[14] In addition to the unprecedented time resolution enabled by such sources, the XUV absorption spectra of molecules and materials possess element and oxidation state specificity provided by the core-to-valence transitions probed. Measurements in the gas phase have provided new insights into fundamental processes, such as the behavior of electronic[15] and vibrational[16] wave packets, bond dissociation,[17] and charge migration.[18] However, some of the most technologically relevant ultrafast phenomena occur in the solid-state, where the application of time-resolved XUV measurements is relatively recent. Attosecond transient absorption spectroscopy (ATAS) is a powerful technique for such studies that provide a probe of the bulk response. In comparison

a)Present address: Max-Planck-Institut für Kernphysik, 69117 Heidelberg, Germany.
b)Authors to whom correspondence should be addressed: dneumark@berkeley.edu and srl@berkeley.edu

with photoemission, ATAS has the strong advantage that the large bandwidth of the XUV pulses does not limit the energy resolution of the experiment. When transitioning ATAS from the gas phase to the bulk solid, new complications arise. In particular, due to the high attenuation of XUV light in materials, samples must generally be on the order of a few tens of nanometers thick, and for the same reason, materials need to be deposited on freestanding ultra-thin membrane substrates such as silicon nitride or diamond. The sample thickness and vacuum conditions required for XUV transmission mean that heat dissipation is poor and predominantly based on 2D transport. As the sample is not constantly refreshed, low damage thresholds and heat buildup mean that the repetition rate of the experiment must also be decreased, the sample has to be rapidly translated, or both of these steps must be taken.

An instrumental case study is presented for dealing with these complications in vanadium dioxide (VO_2), a technologically important material that exhibits a sub-100 fs insulator-to-metal phase transition (IMT).[19–21] When performing time-domain measurements on VO_2 below or around the IMT temperature, it is critical that the sample cools back to a value below its critical temperature (T_c) of 340 K (Ref. 6) between successive pump pulses. Experimentally it is shown that this condition is not met by raster scanning the sample, where the measured response is that of the higher temperature metallic phase. This is due to the relatively slow motion of even fast vacuum translation stages (typical speed of few mm/s), compared to the typically millisecond inter-pulse time of 100 Hz to kHz repetition rate laser systems. While faster stages are available, they generally have limited translation range and a high price point. In this work, a custom sample mount consisting of a rapidly rotating hollow-shaft motor is introduced to provide more rapid sample movement through the laser beam focal volume. This introduces cooled sample sites to each pulse of the laser to overcome the heat dissipation problem. The rapidly rotating hollow-shaft motor design provides a qualitatively different XUV transient absorption response compared to raster scanning measurements; the thermal heat load in the thin-film sample can be dissipated, and the ultrafast response of the insulating phase and the phase transition are captured without artifacts. The detailed physics and time scales measured in VO_2 are described in Ref. 22, whereas this work focuses rather on the technical aspects. Heat transfer simulations are performed using a finite element method in COMSOL 5.2a, verifying that for the given experimental conditions, raster scanning at 1.6 mm/s translational speed is insufficient to counteract the accumulative buildup of heat between subsequent laser pulses, even at a reduced 100 Hz repetition rate of the experiment. Heating issues can be overcome, however, by implementing rapid sample rotation, effectively realizing >170 mm/s translational speed.

II. EXPERIMENTAL OVERVIEW

The experimental apparatus designed for this work is illustrated in Fig. 1. A carrier-envelope phase stable titanium-sapphire laser system (Femtolasers, 1.6 mJ, 1 kHz) is used to pump a neon-filled (2 bars static filling) hollow-core fiber with near-infrared (NIR) pulses, where self-phase modulation broadens the pulse spectrum to a range spanning from approximately 400 to 1000 nm. The pulses are temporally compressed using a chirped mirror compressor consisting of four mirror pairs (Ultrafast Innovations GmbH) and a pair of thin fused-silica glass wedges for finely tuned dispersion control. Pulses can be compressed to sub-5 fs in duration, as characterized via a dispersion scan.[23] The repetition rate is reduced to 100 Hz when required with an in-line optical chopper.

A majority (80%) of the pulse energy is used to generate high-order harmonics in the probe arm. For the VO_2 experiments described in this work, krypton was used as the harmonic generation medium at a backing pressure of ~30 Torr to produce attosecond pulses, optimized for maximum photon flux in the 40-50 eV region and yielding close-to-continuous harmonic spectra. Residual NIR light is filtered out using a 200-nm-thick aluminum filter, and the remaining XUV light is focused through the sample using a toroidal mirror in a 1:2 geometry to achieve a spot size of approximately 70 μm full-width at half maximum (FWHM) at the sample.

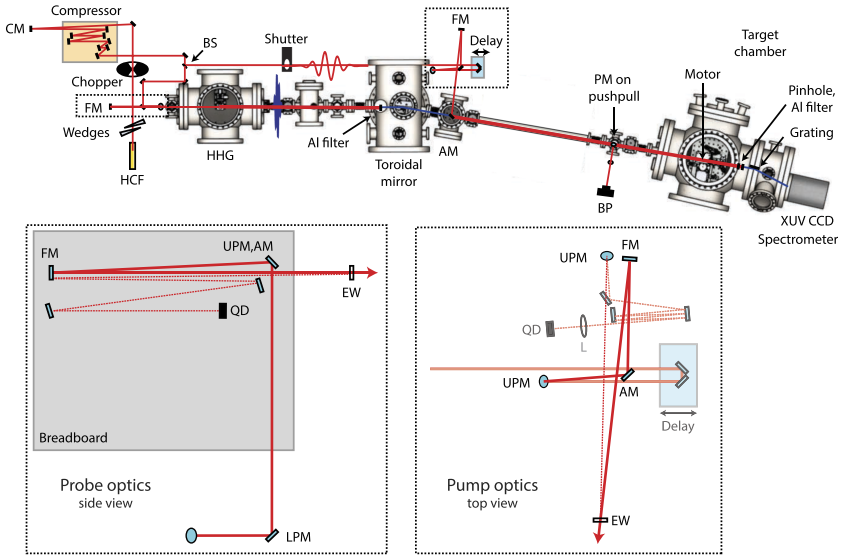

FIG. 1. The beamline for solid-sate XUV transient absorption experiments. NIR light is shown in red, and XUV light is shown in blue. HCF = hollow-core fiber, FM = focusing mirror, CM = collimating mirror, BS = beam splitter, AM = annular mirror, PM = pickoff mirror, and BP = beam profiler. Insets show the probe and pump beam optics, including beam-pointing stabilization. The thinner red line in the insets corresponds to the back reflection from the chamber entrance windows, which is used to perform the stabilization. UPM = upper periscope mirror, LPM = lower periscope mirror, AM = actuated mirror, EW = entrance window, L = lens, and QD = quadrant diode. In the pump optics inset, darker (lighter) colors denote beams and optics in the upper (lower) plane.

After transmission through the VO_2 sample, the XUV probe beam enters the spectrometer through a 200 μm pinhole and an additional 200-nm-thick aluminum filter, and the XUV is spectrally dispersed with a gold coated flat-field variable-line-spacing reflection grating onto an XUV-sensitive CCD camera. The remaining 20% of the pulse energy is used for the pump arm to induce the insulator-to-metal transition, and this pulse undergoes a variable time delay using a piezoelectric stage for fine delays and a motorized linear actuator stage for coarse delays. A broadband half-wave plate in combination with a wire-grid polarizer is used for the attenuation of the pump beam, which is focused and then recombined co-linearly with the probe beam on a 45° annular silver-coated mirror. The pump beam focuses through the sample to approximately 200 μm FWHM and is blocked with the aforementioned pinhole and aluminum filter combination. Measurements are performed in a pump-on pump-off scheme, using an optical shutter in the pump arm, to measure the spectrally resolved absorbance change (ΔOD) in the XUV as a function of time delay.

III. STATIC SAMPLE DIAGNOSTICS

A. Optical static measurements

The target chamber is equipped to measure NIR transmission through the sample and characterize the foci of the pump and probe beams. The chamber geometry in the NIR measurement mode is illustrated in Fig. 2(a). A pickoff mirror on a motorized linear vacuum stage can be moved into the beam path, which sends the pump beam into a visible-NIR spectrometer or onto a power meter. The sample holder is mounted on motorized fast XY translation stages and can be moved to translate between multiple sample and reference slots. Losses along the beam path are calibrated such that absolute pump power at the sample focus can be measured. A pickoff mirror before entering the target chamber can be inserted (see Fig. 1) to send both the attenuated pump and HHG driver beams (aluminum filter removed) onto a beam profiler, with a distance matched precisely to the position of the target sample. In combination with the measured pump beam power, this allows for the determination of absolute fluences as well as setting and assuring spatial overlap of both beams.

Additionally, a quartz halogen heat lamp (12 V, 10 W) is powered by a DC voltage supply and installed adjacent to the sample, at an approximately 1 cm distance, as shown in Fig. 2. Heating the sample *in situ* is critical for characterizing heat sensitive samples. For phase transition materials, measuring the NIR transmission as a function of the lamp voltage provides a direct probe of the switching behavior, where a rapid increase or decrease in transmission can be observed when T_c is crossed. Thin-film samples for absorption measurements are typically deposited on freestanding silicon nitride membranes, which are installed in the same sample holder as a reference. The thin-film VO_2 samples are prepared at a thickness of 25 nm on 30-nm-thick silicon nitride membranes by the method of pulsed laser deposition.[22,24] Except as noted below, the underlying silicon nitride samples by themselves are not found to affect the static or transient spectra of these experiments. In the VO_2 experiments, a 20% change in transmittance of these samples is observed when heating above 340 K, as shown in Fig. 2(b). The critical lamp flux required to induce the phase transition is also used to heat the sample *in situ* to measure the static XUV spectrum of the metallic phase as well as its transient response. Samples were also checked before and after time-resolved experiments to ensure that they still change phase with the same magnitude.

B. XUV static measurements

With the heat lamp on or off, and retracting the NIR pickoff mirror, XUV static absorption spectra can be measured for both the insulating and metallic phases of VO_2, respectively, which can be found in Ref. 22. In semiconductors, heating effects such as bandgap renormalization[25] can also be referenced. High quality static spectra are obtained by using the XY sample stages to alternate rapidly between sample and reference films at the full 1 kHz laser repetition rate, acquiring transmitted XUV spectra over 800 ms and moving to a new position on the membrane surfaces thereafter. Sample thickness, homogeneity, local damage, and defects can be measured by plotting

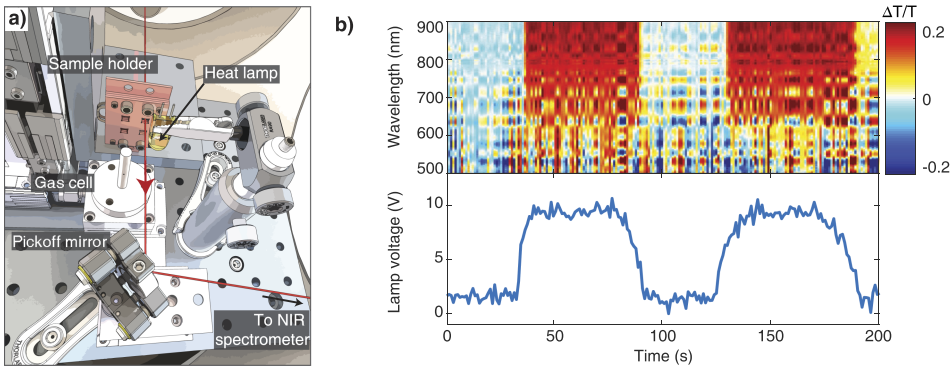

FIG. 2. Target chamber configuration for NIR transmission measurements: (a) the beam passes through a slot in the sample holder and is sent out of the chamber by a pickoff mirror on a motorized stage. Four different positions (e.g., three samples and one reference) on the sample holder can be accessed using the XY stages. (b) Spectrally resolved NIR transmission measurement showing switching behavior of a VO_2 sample upon heating with a quartz heat lamp. Fluctuations on the order of 0.1 ΔT/T are present at wavelengths below 700 nm related to fluctuations in the NIR spectrum, predominantly in regions corresponding to minima in the transmission spectrum. The NIR spectrum of the pulse can be found in Ref. 22.

a transmission map of the integrated XUV signal as a function of the 2D position on the sample surface. Prolonged XUV exposure does lead to increased absorption over time in silicon nitride films, which creates a dark spot in the transmission map where the XUV light has been impinging. Taking optical spectra did not result in similar damage, so it is likely that ionizing radiation damage from the interaction with the XUV radiation is the source of this problem, possibly related to interaction with residual gas in the vacuum chamber environment. A full understanding of the damage mechanism is beyond the scope of this paper; however, based on its observation, samples are always raster scanned even when taking static XUV measurements, and in this way, high quality and reproducible results are obtained.

IV. SPATIAL AND TEMPORAL STABILIZATION FOR 48-h MEASUREMENTS

The high attenuation of XUV light through solid-state samples and yet relatively smaller ΔOD signals compared to the gas phase, together with the decreased repetition rates that must be used, means that acquiring transient absorption spectrograms with sufficient signal-to-noise (i.e., requisite noise level of 2-3 mΔOD for a typical 10-15 mΔOD transient absorption signal change) can take up to 48 h. Since both long-term temporal and spatial drifts can be significant on these time scales, beam-pointing stabilization and time-delay correction are necessary.

Single-point beam-pointing stabilization, where two angular coordinates of the beam are controlled in order to fix its location to a specific spot in the focal plane, is used in both the pump and probe arms to compensate for spatial drifts. The beam-pointing stabilization optics are shown in the insets of Fig. 1. The stabilization ensures that the pump and probe beams remain centered and overlapped at the same point in space. Positional drifts are measured from the back reflection from the chamber entrance windows and are corrected using a single quadrant diode in each arm at a distance precisely matched with the distance to the focus. Active closed-loop control is implemented with an additional sample-and-hold circuit so that the beam positions do not drift between laser pulses for low-repetition-rate experiments or when the pump beam is periodically blocked in pump-on/pump-off measurements. In the probe arm, the upper periscope mirror before the HHG focusing mirror is actuated. The beam is stabilized to the HHG focus using a back reflection from the chamber entrance window that is directed and focused onto a four-quadrant photodiode at a matched distance to the target. In the pump arm, the plane mirror before the focusing mirror is actuated and the back reflection from the entrance window is used to stabilize the beam to the sample focus in the same manner. An output from the amplifier timing unit is used to trigger the beam-pointing stabilization system at repetition rates below 300 Hz, where a digital delay generator is used to shape the proper square-wave amplitude and duration for triggering.

Interferometric stabilization of the key points of the apparatus is a typical way to achieve timing stability, but active stabilization[26,27] by means of a co-propagating continuous wave blue laser is challenging in this case because of the challenges of the low repetition rate, the periodic blocking of the pump arm, and the possibility for residual blue light to be absorbed by successive heating or damage occurring in the solid-state samples. Instead, periodic measurements are performed in neon gas, which has the advantage that (in addition to compensating for time-delay drifts over the course of the measurement) absolute time-zero can be measured and the pulse can be characterized. Measurements in neon are performed between scans, approximately every 8 min, by moving the solid-state sample out of the beam path and inserting a gas cell into the focus using motorized stages [see Fig. 2(a) for a design illustration of the target geometry]. Using the gas cell, a transient absorption measurement can be performed in neon gas at a backing pressure of 100 Torr. The neon response allows an *in situ* determination of both time-zero and the instrument response function,[28] which is then used to retroactively correct time-delay drifts and synchronize scans in the data analysis.[29] A representative time-delay drift trace is shown in Fig. 3, where the experimental measurement is shown in panel (a), zoomed in about the $2s^1 2p^6 4p$ line at 47.1 eV. A lineout is taken over

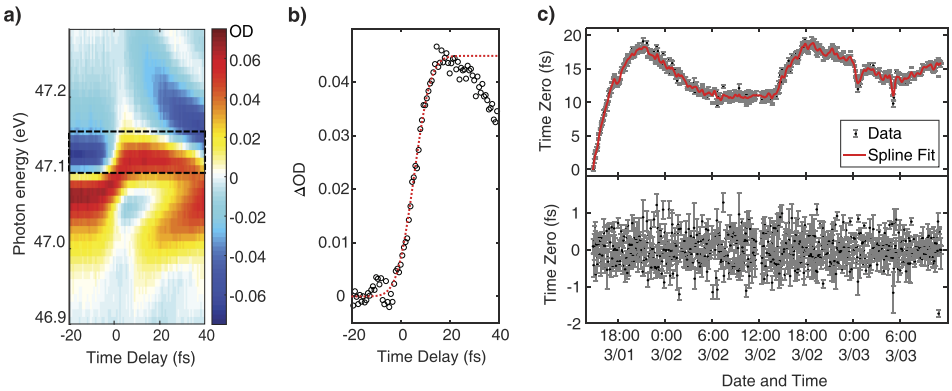

FIG. 3. (a) A representative transient absorption measurement in neon about the $2s^1 2p^6 4p$ absorption line, showing a characteristic lineshape change. For time-delay synchronization, a lineout is taken over the indicated region (black dashed box) as shown in panel (b). The initial rise is fit to an error function, the central position of which is used to quantify time-delay drifts. (c) A representative time-delay drift measurement over a 48-h period, where the upper panel shows the drift in time-zero over the course of a measurement and the lower panel shows the error in the time-zero determination following data correction, with a variance (corresponding to a timing jitter) of 595 as.

the indicated region and fit to an error function, as shown in panel (b), which can be done for each measurement to give the time-delay drifts shown in panel (c). The corrected scan has a variance corresponding to a timing uncertainty of 595 as. This uncertainty is not a fundamental limit but depends on how frequently the time-zero measurements are performed and the time-delay sampling used (in this case 0.1 μm steps, which corresponds to 670 as delays). The instrument response function can be characterized by fitting the lineshape as a function of time delay, as in Ref. 28, and values on the order of 5-7 fs are typically obtained.

V. SAMPLE RASTER SCANNING AND ROTATION

Using the same sample holder as for static spectral measurements, NIR-pump XUV-probe transient absorption measurements can be performed. To mitigate heat buildup and sample damage, the XY stages are used to raster scan across the sample surface. However, as will be shown, this is not sufficient particularly for heat sensitive samples. The stages used (P.I. VT-80, high vacuum version) move at a maximum speed of 1.6 mm/s[30] or a maximum distance of 16 μm between each laser pulse when operating at 100 Hz, which is small compared to the 200 μm FWHM pump beam focal size but is on the faster end of commercially available linear vacuum translation stages. The small sample sizes (typically few mm × few mm freestanding thin-film apertures at most) make more rapid translation with linear stages nearly impossible, especially when considering acceleration/deceleration times. The experiment was programmed such that the stage moved over a 5 × 5 grid of positions across the sample surface, pausing at each location for pump off, shutter opening, and subsequent pump-on measurements. An exposure time of 1 s was used for the VO_2 experiments. Shorter exposures may lead to less heat buildup but significantly reduce the duty cycle of the measurements and require longer experimental run times. As will be shown below, in a scheme solely based on raster scanning, even when moving at maximum speed during each 1-s accumulation time, it is not feasible for the VO_2 sample to relax below T_C between each subsequent laser pulse. Thus a more sophisticated motion of the sample needs to be employed since any further reduction of the repetition rate (e.g., 10 Hz requiring 480 h of data acquisition time) is impractical.

With this in mind, an alternate sample holder was designed to make a measurement of the IMT dynamics possible, where samples are mounted centered on and normal to the axis of a vacuum-compatible hollow-shaft motor (Koford Engineering), as illustrated in Fig. 4. The motor is encased in an aluminum housing to dissipate heat and attaches to the XY translation stages. Rotation speeds up to 10 000 rpm or 167 Hz can be achieved. For the VO_2 experiments, the stages were positioned such that the beams impinged at a radius of 0.75 mm from the central axis of the hollow shaft and the motor was operated at 37 Hz. This corresponds to a velocity of >170 mm/s, or slightly over one full rotation of every three laser pulses when operating at 100 Hz, much greater than can be achieved with linear stages. The motor frequency is out of phase with the laser repetition rate such that the same areas on the sample are not irradiated repeatedly. Additionally, the motor housing was fabricated with a transmission hole to allow for measurements bypassing the sample. For example, measurements through a gas cell can be performed, as shown in Fig. 4(b), for the time-zero reference measurements. A close-up of the sample mounting is shown in Fig. 4(c) (Multimedia view), where the long screws are used as handles for easily exchanging the sample without removing the entire housing from the chamber.

VI. EXPERIMENTAL MEASUREMENTS ON VO_2

Transient NIR-pump XUV-probe absorption experiments were performed on VO_2 thin films at 100 Hz at a NIR pump fluence of 25 mJ/cm^2, with a pump beam focal spot size of 200 μm FWHM. As noted, samples were 25 nm thin films of polycrystalline VO_2[31] deposited on 30 nm freestanding silicon nitride membranes. The freestanding membrane area was 3 mm × 3 mm, and the membrane was supported on a

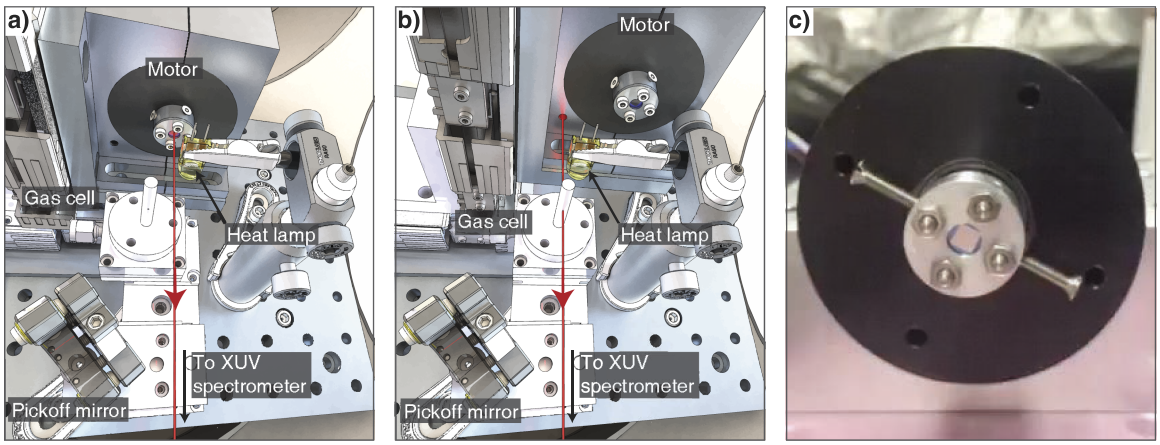

FIG. 4. Target chamber setup for transient absorption measurements. (a) The beam transmits through the sample mounted on the hollow-shaft motor and goes straight to the XUV spectrometer. (b) The stages are moved such that the beam transmits through a hole in the motor housing and passes through the gas cell for time-zero reference measurements. The cell can also be moved out of the beam path for optimizing the XUV harmonic flux. (c) A close-up of the sample holder cap that is attached to the motor. Multimedia view: https://doi.org/10.1063/1.4994041.1

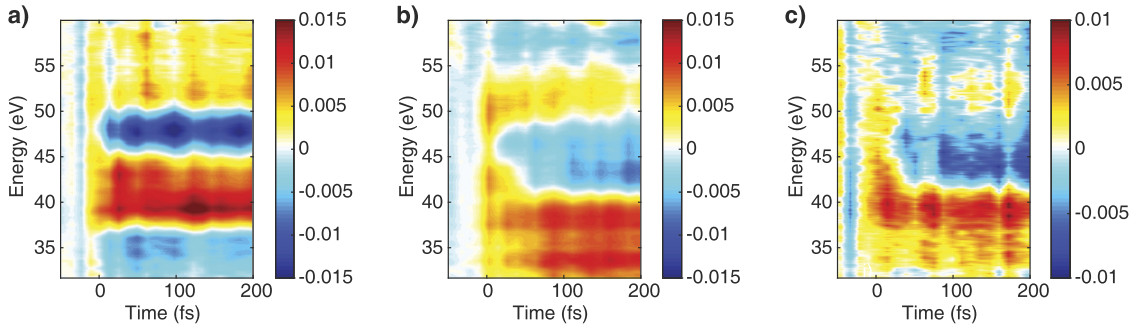

FIG. 5. Transient absorption spectrograms for VO_2 with (a) rotating sample with no heat, (b) rotating sample with the heat lamp on, and (c) raster scanned sample with no heat. In (c), the negative time-delay signal is subtracted for straightforward comparison. The negative time-delay signal was taken as the average XUV absorption spectrum from −10 to −50 fs, and this signal was subtracted across all time delays. The subtracted spectrum had peak magnitudes on the order of 10 mΔOD and the spectral shape resembled the changes observed upon heating. All measurements were performed at a fluence of 25 mJ/cm^2.

silicon frame of 7.5 mm × 7.5 mm outer dimensions, 3 mm × 3 mm aperture, and 525 μm thickness. The experiment was performed with the hollow-shaft motor installed, operating at a rotation speed of 37 Hz and with a radius of 0.75 mm between the beam and motor axis. The experiment was performed first on the sample with no heating and then with the heat lamp on to thermally induce the insulator-to-metal phase transition.

The resulting XUV transient absorption spectrograms (nominally 800 nm excitation with sufficient power density to induce the insulator-to-metal transition and XUV probing) with sample rotation are shown in Fig. 5, depicting the qualitatively different behavior between the insulating phase (a) and the metallic phase (b) and providing evidence that the sample is able to cool below T_C between successive laser pulses. The measurements were also obtained using the raster scanning method described in Sec. V. The resulting spectrogram (c) is identical to the measurement with the heat lamp on, indicating that it is the response of the metallic phase. Indeed, the raster scanning experiment showed the same result when performed with the heat lamp on and heat lamp off. A non-zero signal at negative time delays was also observed in the latter case, showing that the preceding pulse 10 ms prior still had some effect on the XUV spectrum, additionally verifying the problems with laser-induced heating effects. Comparison with the heating lamp measurement confirmed that these changes were indeed a result of the phase transition, as opposed to alternative heating-induced semiconductor effects, such as phonon-induced renormalization of the bandgap, which can sometimes be observed in laser-heated samples at negative time delays.[32] All these observations make clear that raster scanning with linear translation stages is not sufficient to counteract accumulative heating: the sample does not cool below *Tc* between successive laser pulses, even at the reduced 100 Hz repetition rate. The rotating sample measurements, in contrast, allow for probing the true ultrafast response of the insulating phase. A detailed analysis of the physics of the insulating and metallic phase experiments and the verification of the IMT via a fluence-dependent measurement can be found in Ref. 22. Measurements at 1 kHz, even with sample rotation, resulted in measuring the response of the metallic phase as well as permanent sample damage, where thermal switching could no longer be observed.

VII. SIMULATIONS: HEAT DISSIPATION IN THIN FILMS

To validate our interpretation of the experimental results and estimate the rate of heat buildup for each case more quantitatively, time-dependent heating simulations were performed using finite element analysis in COMSOL 5.2a. The sample geometry was defined as a VO_2 layer of 7.5 mm × 7.5 mm × 25 nm thick dimensions on a silicon nitride layer of 7.5 mm × 7.5 mm × 30 nm thick dimensions on a silicon frame of 7.5 mm × 7.5 mm outer dimensions, 3 mm × 3 mm square aperture, and 525 μm thickness, in accordance with the sample geometry. For the simulation, the grid elements were generated using a triangular mesh swept through each layer, with a finer mesh used for the freestanding area and a coarser mesh used for the area over the frame. The silicon frame was treated with thermally insulating boundaries and acted as an effective heat sink. The exposed membrane surfaces (7.5 mm × 7.5 mm VO_2 area and 3 mm × 3 mm Si_3N_4 area) were modeled with blackbody radiation described by the Stefan-Boltzmann law (COMSOL diffuse surface module). Convective heat dissipation is absent under the vacuum conditions employed here. The emissivity and other material properties used are listed in Table I. The material properties of the *insulating* phase of VO_2 were used for the heat capacity, density, and NIR penetration depth (to reflect the initial absorption process), and the *metallic* phase value was used for the emissivity and

TABLE I. VO_2, Si_3N_4, and Si material properties for heat transport.

Parameter	VO_2 (ins.)	VO_2 (met.)	Si_3N_4	Si
Heat capacity, C_p [J/(g·K)]	0.66[34,35]	0.78[34,35]	0.7[36]	0.705[37]
Thermal conductivity, κ [W/(m·K)]	6.5[35]	6.5[35]	13[36,38]	156[39]
Emissivity, ε	0.09[40,a]	0.35[40,a]	0.005[41,a]	0.12[42]
Penetration depth at 800 nm (nm)	120[43]	90[43]	...	...
Density, ρ (g/cm^3)	4.57[44]	4.65[44]	3.2[36]	2.33[37]

[a]Values for VO_2 and Si_3N_4 are specifically for thin films of 25 and 30 nm thickness, respectively.

thermal conductivity (to reflect the cooling process occurring predominantly in the final state). The enthalpy of the phase change is 4.23 kJ/mol,[33] which corresponds to 0.58 mJ/cm^2 given the molar mass, density, and thickness of the VO_2 samples, and this factor could be neglected.

A periodic heat flux into the sample was implemented using a Gaussian beam profile with a 200 μm full-width at half-maximum and a fluence of 25 mJ/cm^2, matching the experimental conditions. In the beam propagation direction normal to the sample surface, an exponentially decaying thermal distribution was used for Beer's law absorption into the VO_2 layer, using the penetration depth of the insulating phase at 800 nm. Si_3N_4, a wide-bandgap material, was treated as non-absorbing with no incident heat flux. The temporal pulsed behavior was modeled with a rectangular waveform with a period of 10 ms and a pulse duration of 0.1 ms. For the heating dynamics, the femtosecond pulse duration is not important as long as the pulse energy is deposited in a short time compared to the limiting rate of cooling—in this case, shorter pulse durations than specified above were shown to have no effect. For the raster scanning case, the Gaussian heat source was defined at a starting position of 0.75 mm from the sample center, and the sample was translated linearly at 1.6 mm/s using a moving mesh. For the rotating motor case, the Gaussian heat source was placed at an offset of 0.75 mm to the sample center and a moving mesh was used to rotate the material relative to the spatial frame at 37 Hz. Time-dependent simulations were carried out from 0 to 30 ms with a step size of 1 ms, with a solver convergence tolerance of 0.01, and using explicit events to sample across the laser pulse duration (τ) at $-\tau/5$, 0, $\tau/5$, $2\tau/5$, $3\tau/5$, $4\tau/5$, $5\tau/5$, and $6\tau/5$ relative to the pulse start time. Snapshots of the temperature profile on the sample surface are illustrated in Fig. 6 (Multimedia view), which follow the heat dissipation of an incident pulse in the steady state limit.

A global temperature probe was defined, which tracks the temperature in the focal volume for raster scanning (in the sample center) and rotating sample geometries (at a radial offset of 0.75 mm). A plot of the temperature in the focal volume over the course of ten laser pulses is shown in Fig. 7,

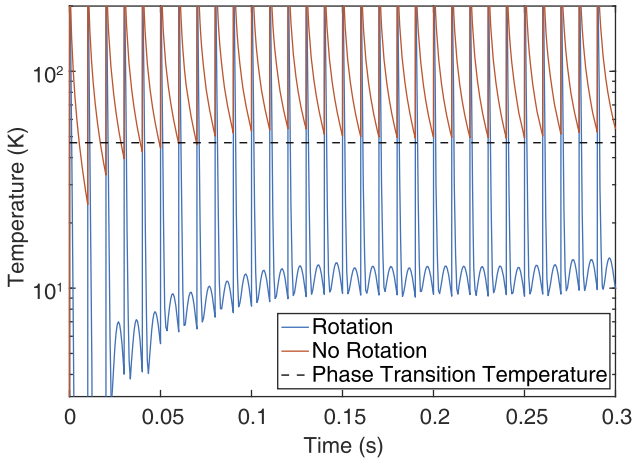

FIG. 7. Temperature change in the focal volume of the laser is plotted on a logarithmic scale for the case of raster scanning with sample rotation (blue) and without sample rotation (orange). Small local maxima in the rotating sample data correspond to a previously irradiated part of the sample passing through the focal volume.

comparing each case. As can be seen in the figure, in the no-rotation case, the temperature in the focal volume just before each pulse climbs above T_C within six pulses, or 60 ms, even when the sample is translated continuously and at maximum speed with the linear stages. After the first six pulses, all subsequent pulses probe the response of metallic VO_2 as opposed to the insulating phase of VO_2, not sampling the IMT process. Thus, for a typical exposure time of 1 s, accumulating signal over 100 laser pulses, only 6% of the acquired XUV absorption signal would reflect the transient response of the insulating phase. In the rotating sample case on the other hand, the temperature in the focal volume reduces rapidly and in fact remains within 10 K of the starting room-temperature value preceding each laser pulse, thus providing an accurate probe of the response of the insulating phase.

The presented results show the optimal case of raster scanning, where the stage is continuously moving, which is still insufficient for thin-film VO_2 samples in a 100 Hz

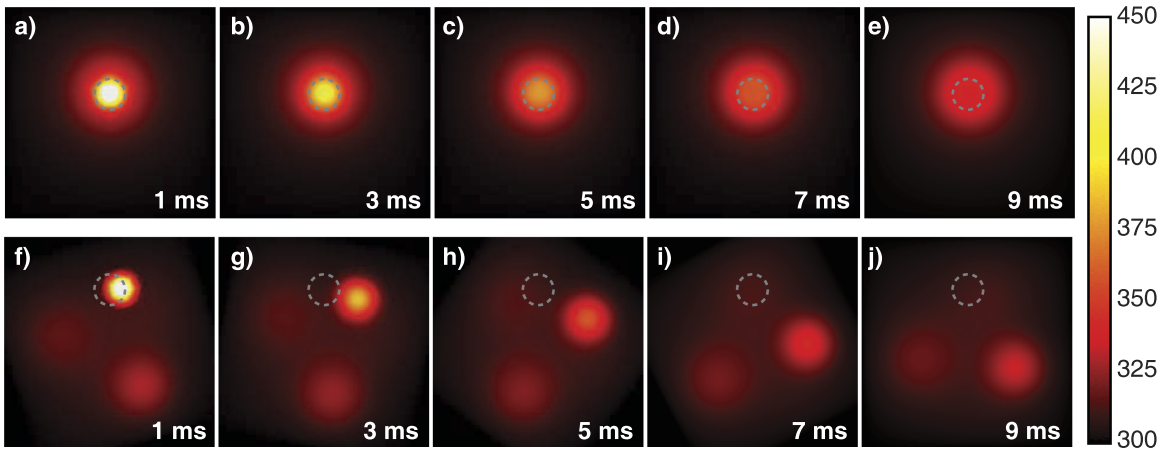

FIG. 6. Snapshots of the temperature profile on the sample surface for sample raster scanning [(a)–(e)] and sample rotation [(f)–(j)] in the steady state limit, following the dissipation of heat in a 100 Hz experiment, over the 10 ms period between incident laser pulses. The focal volume of the laser where the next pulse will impinge is marked in dashed gray. Multimedia views: https://doi.org/10.1063/1.4994041.2; https://doi.org/10.1063/1.4994041.3

experiment. In most experiments, the stage is paused at each position on the sample for some time, leading to even higher temperature buildup. Some supplementary cooling can be provided by other methods, e.g., introducing a flow of inert and XUV transparent gas over the front and back surfaces of the sample for convective cooling, cooling the ambient surroundings to act as a blackbody heat sink, using a gridded substrate such as a TEM grid, and sending the beam between the thermally conductive bars or coating VO_2 on a thin layer of an inert, more thermally conductive material such as diamond. However, particularly for samples with pulse-to-pulse sensitivity, rapid sample rotation represents a clean way to get injected heat out of the focal volume, and it results in no loss in the signal. The motor frequency used in this work is not a unique solution, and in general, it should be based on the consideration of Eq. (1), where f_{rot} and f_{rep} are the motor rotation frequency and laser repetition frequency, respectively, r is the radius of rotation, d_{beam} is the beam diameter, and n is the desired integer number of beam diameters between pulses,

$$2\pi \times r \times (f_{rot}/f_{rep}) \geq n \times d_{beam}. \quad (1)$$

The motor frequency used in the presented experiment corresponds to 10 d_{beam} between subsequent pulses, although a lower frequency could certainly be used in this case. The motor frequency should also ideally be out of phase with the repetition rate to maximize the time before the same sample area is irradiated again. For even more sensitive samples, linear motion can be combined with rapid sample rotation to spiral over the sample surface, and if possible sample size can be increased, which would allow for working at a larger radius and possibly even higher repetition rates. Whether such measures are necessary depends on the specific thickness-dependent thermal properties of the sample under investigation.

VIII. CONCLUSIONS

An attosecond transient absorption beamline is presented that is tailored to investigate thin-film samples and nanostructures, utilizing a rotating sample mount to mitigate heat buildup. The system is capable of stabilizing measurements to sub-femtosecond resolutions for up to 48-h experiments. Sensitive diagnostics are included for measuring high quality static XUV and NIR transmission spectra, both at room temperature and for samples heated *in situ*, as well as characterizing fluences and pump beam power incident on the sample.

The presented experimental and simulated data on vanadium dioxide demonstrate the care that must be taken in such measurements and the necessity of going beyond raster scanning when working with truly heat sensitive samples. While some of the elements of this apparatus are specific to XUV measurements, the conclusions regarding heat transport are general to thin-film samples in vacuum. The hollow-shaft motor scheme presented demonstrates one way of mitigating these effects. While such measures may not be required for higher thermal conductivity samples such as silicon or generally thicker samples, it is critical to consider the thermal properties of the system being investigated and the reversibility or irreversibility of the process at hand.

ACKNOWLEDGMENTS

We would like to acknowledge helpful discussions with Mihai Vaida as well as Eric Granlund and the UC Berkeley College of Chemistry machine shop. The work of M.F.J., C.J.K., and C.O. was supported by the DARPA PULSE program (No. W31P4Q-13-1-0017) and that of P.M.K. by a MURI grant from the AFOSR (No. FA9550-15-1-0037), with equipment provided by The Office of the Assistant Secretary of Defense for Research and Engineering through a NSSEFF grant, and the W. M. Keck Foundation and the Department of Energy (No. DE-AC03-76SF00098). M.F.J. gratefully acknowledges additional fellowship support from the University of California, Berkeley and LAM Research; C.O. is grateful for support from the Humboldt Foundation, and P.M.K. acknowledges support from the Swiss National Science Foundation.

[1] K. Nasu, *Photoinduced Phase Transitions* (World Scientific Publishing Co. Pte. Ltd., 2004).
[2] D. N. Basov, R. D. Averitt, D. van der Marel, M. Dressel, and K. Haule, "Electrodynamics of correlated electron materials," Rev. Mod. Phys. **83**, 471 (2011).
[3] Y. Tokura and N. Nagaosa, "Orbital physics in transition-metal oxides," Science **288**, 462–468 (2000).
[4] A. J. Millis, B. I. Shraiman, and R. Mueller, "Dynamic Jahn-Teller effect and colossal magnetoresistance in $La_{1-x}Sr_xMnO_3$," Phys. Rev. Lett. **77**, 175–178 (1996).
[5] J. G. Bednorz and K. A. Müller, "Possible high T_c superconductivity in the Ba–La–Cu–O system," Z. Phys. **64**, 189–193 (1986).
[6] F. J. Morin, "Oxides which show a metal-to-insulator transition at the Neel temperature," Phys. Rev. Lett. **3**, 34–36 (1959).
[7] M. Imada, A. Fujimori, and Y. Tokura, "Metal-insulator transitions," Rev. Mod. Phys. **70**, 1039–1263 (1998).
[8] Z. Yang, C. Ko, and S. Ramanathan, "Oxide electronics utilizing ultrafast metal-insulator transitions," Annu. Rev. Mater. Res. **41**, 337–367 (2011).
[9] H. T. Kim *et al.*, "Mechanism and observation of Mott transition in VO_2-based two- and three-terminal devices," New J. Phys. **6**, 52 (2004).
[10] T. Driscoll, H. T. Kim, B. G. Chae, M. Di Ventra, and D. N. Basov, "Phase-transition driven memristive system," Appl. Phys. Lett. **95**, 43503 (2009).
[11] K. Ramasesha, S. R. Leone, and D. M. Neumark, "Real-time probing of electron dynamics using attosecond time-resolved spectroscopy," Annu. Rev. Phys. Chem. **67**, 41–63 (2016).
[12] G. Farkas and C. Tóth, "Proposal for attosecond light pulse generation using laser induced multiple-harmonic conversion processes in rare gases," Phys. Lett. A **168**, 447–450 (1992).
[13] M. Ferray *et al.*, "Multiple-harmonic conversion of 1064 nm radiation in rare gases," J. Phys. B: At., Mol. Opt. Phys. **21**, L31–L35 (1988).
[14] F. Krausz and M. Ivanov, "Attosecond physics," Rev. Mod. Phys. **81**, 163–234 (2009).
[15] O. Smirnova *et al.*, "High harmonic interferometry of multi-electron dynamics in molecules," Nature **460**, 972–977 (2009).
[16] W. Li *et al.*, "Time-resolved dynamics in N_2O_4 probed using high harmonic generation," Science **322**, 1207 (2008).
[17] L. Nugent-Glandorf, M. Scheer, D. A. Samuels, V. M. Bierbaum, and S. R. Leone, "Ultrafast photodissociation of Br_2: Laser-generated high-harmonic soft x-ray probing of the transient photoelectron spectra and ionization cross sections," J. Chem. Phys. **117**, 6108 (2002).
[18] P. M. Kraus *et al.*, "Measurement and laser control of attosecond charge migration in ionized iodoacetylene," Science **350**, 1525–1529 (2015).
[19] A. Cavalleri, T. Dekorsy, H. H. W. Chong, J. C. Kieffer, and R. W. Schoenlein, "Evidence for a structurally-driven insulator-to-metal transition in VO_2: A view from the ultrafast timescale," Phys. Rev. B **70**, 161102 (2004).
[20] D. Wegkamp *et al.*, "Instantaneous band gap collapse in photoexcited monoclinic VO_2 due to photocarrier doping," Phys. Rev. Lett. **113**, 216401 (2014).
[21] B. T. O'Callahan *et al.*, "Inhomogeneity of the ultrafast insulator-to-metal transition dynamics of VO_2," Nat. Commun. **6**, 6849 (2015).

[22]M. F. Jager *et al.*, "Tracking the insulator-to-metal phase transition in VO_2 with few-femtosecond extreme UV transient absorption spectroscopy.," Proc. Natl. Acad. Sci. U. S. A. **114**, 9558–9563 (2017).
[23]M. Miranda *et al.*, "Characterization of broadband few-cycle laser pulses with the d-scan technique," Opt. Express **20**, 18732 (2012).
[24]J. Nag, "The solid-solid phase transition in vanadium dioxide thin films: Synthesis, physics and applications," Ph.D. dissertation (Vanderbilt University, 2011).
[25]A. Walsh, J. L. F. Da Silva, and S. H. Wei, "Origins of band-gap renormalization in degenerately doped semiconductors," Phys. Rev. B **78**, 1–5 (2008).
[26]M. Chini *et al.*, "Delay control in attosecond pump-probe experiments," Opt. Express **17**, 21459 (2009).
[27]M. Sabbar *et al.*, "Combining attosecond XUV pulses with coincidence spectroscopy," Rev. Sci. Instrum. **85**, 103113 (2014).
[28]A. Blättermann *et al.*, "*In situ* characterization of few-cycle laser pulses in transient absorption spectroscopy," Opt. Lett. **40**, 3464 (2015).
[29]T. Ding *et al.*, "Time-resolved four-wave-mixing spectroscopy for inner-valence transitions," Opt. Lett. **41**, 709–712 (2016).
[30]Motion Control Vacuum Catalog–PIlmiCos Motion Control Vacuum Catalog: PIlmiCos (2014).
[31]J. Nag and R. F. Haglund, Jr., "Synthesis of vanadium dioxide thin films and nanoparticles," J. Phys.: Condens. Matter **20**, 264016 (2008).
[32]M. Zürch *et al.*, "Direct and simultaneous observation of ultrafast electron and hole dynamics in Germanium," Nat. Commun. **8**, 15734 (2017).
[33]J. C. Rakotoniaina *et al.*, "The thermochromic vanadium dioxide: I. Role of stresses and substitution on switching properties," J. Solid State Chem. **103**, 81–94 (1993).
[34]G. V. Chandrashekhar, H. L. C. Barros, and J. M. Honig, "Heat capacity of VO_2 single crystals," Mater. Res. Bull. **8**, 369–374 (1973).
[35]C. N. Berglund and H. J. Guggenheim, "Electronic properties of VO_2 near the semiconductor-metal transition," Phys. Rev. **185**, 1022–1033 (1969).
[36]G. Ziegler, J. Heinrich, and G. Wötting, "Relationships between processing, microstructure and properties of dense and reaction-bonded silicon nitride," J. Mater. Sci. **22**, 3041–3086 (1987).
[37]D. R. Lide, "Properties of the elements and inorganic compounds; physical constants of inorganic compounds," in *CRC Handbook of Chemistry and Physics*, 84th ed. (CRC Press, 2003).
[38]X. Zhang and C. P. Grigoropoulos, "Thermal conductivity and diffusivity of free-standing silicon nitride thin films," Rev. Sci. Instrum. **66**, 1115–1120 (1995).
[39]C. J. Glassbrenner and G. A. Slack, "Thermal conductivity of silicon and Germanium from 3°K to the Melting point," Phys. Rev. **134**, A1058–A1069 (1964).
[40]F. Guinneton, L. Sauques, J.-C. Valmalette, F. Cros, and J.-R. Gavarri, "Optimized infrared switching properties in thermochromic vanadium dioxide thin films: Role of deposition process and microstructure," Thin Solid Films **446**, 287–295 (2004).
[41]P. J. Van Zwol *et al.*, "Emissivity of freestanding membranes with thin metal coatings, e-print arXiv: 151106111 (2015).
[42]P. J. Timans, "Emissivity of silicon at elevated temperatures," J. Appl. Phys. **74**, 6353–6364 (1993).
[43]A. Cavalleri *et al.*, "Picosecond soft x-ray absorption measurement of the photoinduced insulator-to-metal transition in VO_2," Phys. Rev. B **69**, 153106 (2004).
[44]H. Wen *et al.*, "Structural and electronic recovery pathways of a photoexcited ultrathin VO_2 film," Phys. Rev. B **88**, 165424 (2013).